# Chapter 4

# Modification & Analysis

*What will prove altogether remarkable is that some very simple schemes to produce erratic numbers behave identically to some erratic aspects of natural phenomena*
Mitchell Feigenbaum, 1980

Visually, the bubbling experiment was really beautiful to observe. From a single steady train of pearly bubbles at higher periodicities, to a sequence of alternating bubble sizes and finally a flurry of bubbles when the system goes into chaos. The dynamics of this system needed to be understood and analyzed before trying to control the bubbling phenomenon. This called for visualizing the system in various subspaces, reading the underlying order of the bubble sizes and finally crystallizing all the observations into a control algorithm. This section deals with the deductions made from the experimental data.

## 4.1. Formation of a single bubble

As a bubble is produced, the pressure in the gas inlet upstream changes. Therefore the line pressure in the gas stream can characterize bubbling. The output of the pressure transducer

measuring the pressure upstream of the nozzle was fed to the computer through a DAQ card and the pressure trace seen with LabView in real-time as the bubble is being formed. As a bubble is formed, the pressure in the gas inlet begins to decrease. A typical bubble formation pressure trace is shown in the **figure. 4.1**

It is observed that the pressure rises rapidly, reaches a peak and then begins to fall off at a much slower rate than the rate of pressure increase. When a bubble is just beginning to form, the nozzle orifice is covered with a film of liquid which seals the orifice and thus does not allow the gas to form the bubble (figure 4.1, region 1). The surface tension forces prevent the seal from breaking and so the pressure in the gas inlet line rises. When the pressure in the gas line exceeds the surface tension forces of the liquid, the seal breaks and the bubble begins to form. As the liquid seal breaks (figure 4.1, region 2), the gas pressure drops and as the bubble begins to grow (Figure 4.1, region 3), the gas pressure drops even further. The bubble grows upto a point when the the buoyancy forces exceed the surface tension forces holding the bubble down to the nozzle face. Once the buoyancy force exceeds the surface tension forces (figure 4.1, region 4), bubble release occurs and a liquid seal forms at the nozzle orifice. This marks the formation of another bubble and the whole cycle repeats again. So the bubble starts forming when the pressure in the line is maximum. The pressure slowly starts falling as the bubble is formed and when bubble release occurs, pressure is at the lowest point in the line. It can be observed that the initial rate of decrease of pressure is much higher than the rate of decrease of pressure near bubble release. This happens because the initial rate of growth of the bubble is rapid and as the bubble reaches the maximum volume dictated by the surface tension of the liquid, the growth of the bubble is inhibited and is slower.

Another phenomenon which was observed was that of 'shoulders' in the experimental data. It was found that the pressure time series peaks were 'interrupted' with smaller shoulders which has

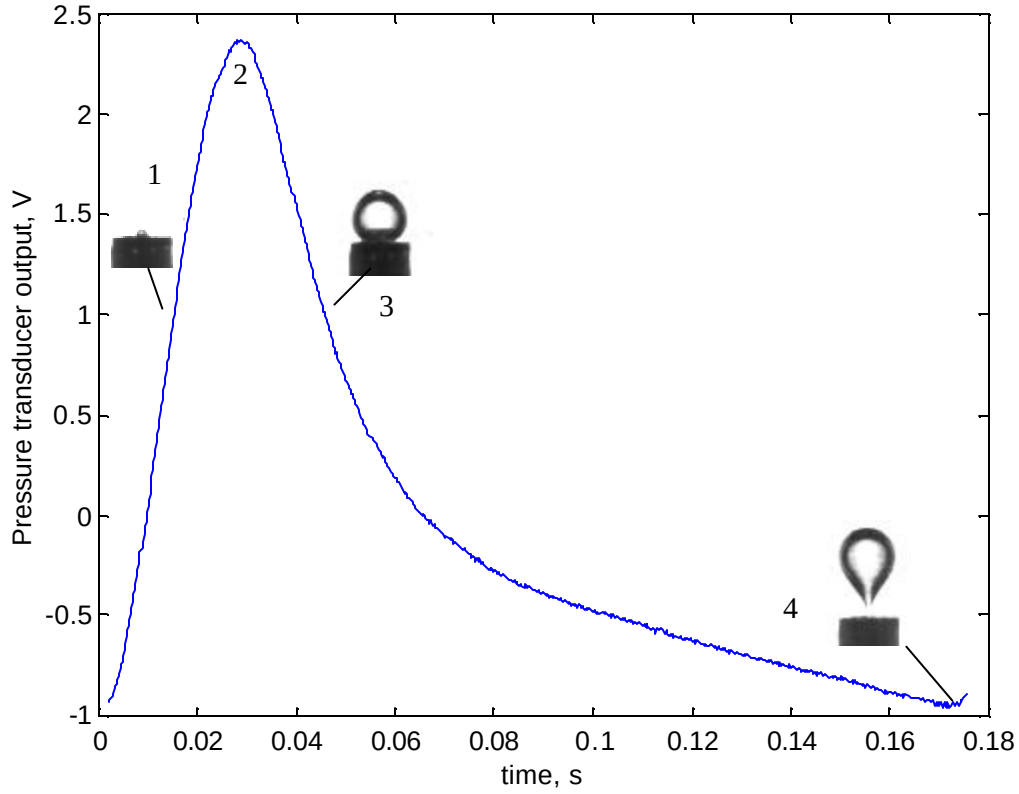


Figure 4.1. Pressure trace in gas inlet line, upstream of the nozzle. (1) surface tension forces are larger than the pressure in the nozzle, preventing bubble growth;(2) pressure in nozzle equals surface tension forces; (3) bubble growth occurs; and (4) buoyancy and inertial forces overcome surface tension, causing bubble detachment.

lower peak heights, but could not be neglected in the period calculations. A typical 'shoulder' occurrence is shown in **figure 4.2**.

On further investigation with high-speed imaging, it was found that there is indeed a physical phenomenon associated with the occurrence of these shoulders. It can be seen from figure 4.2 that the 'shoulder' occurs after a series of medium to large sized bubbles. When the bubble just before the 'shoulder' leaves the nozzle tip, due to its large size the bubble creates a wake around itself. This causes the succeeding bubble to get sucked into the wake and causes it to leave before it matures into a larger bubble. This prematurely released bubble then coalesces with the preceeding bubble, after which the next bubble does not get affected by any wake and thus is large. The phenomenon of shoulders was mainly predominant near period-4 regime, close to the occurrence of chaos. The 'shoulders' were ignored in analysis because the peak-finding algorithm was configured to detect major peaks only.

## *4.2. Regimes of bubbling*

With a single train of bubbles, bubbling regimes having periodicities of 1 through 8 have been reported before entering the regime of chaotic bubbling. With glycerol solutions, bubbling regimes of 1,2,4 and 8 have been reported (Cheng, 1996). With the present study, bubbling regime of 8 was not observed. This is attributed to the larger size of the nozzle used as compared to previous investigation by Cheng (1996), where a nozzle diameter of 1mm ID was used. The bubbling system was seen to undergo a period doubling bifurcation into chaos. This section reproduces results by previous workers by observing the bifurcation sequence of bubbling with increase in flow rate.

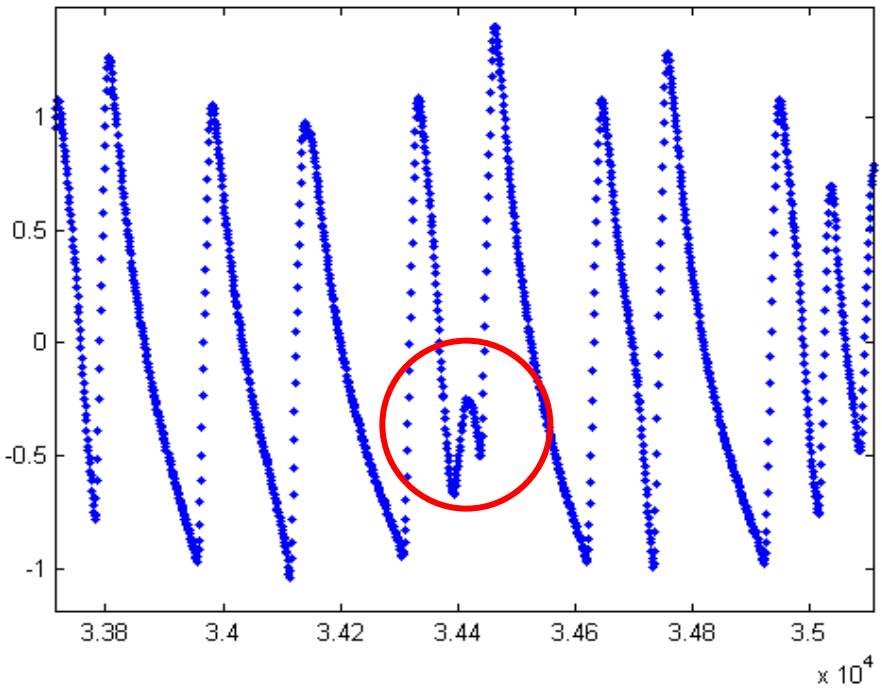


Figure 4.2. 'Shoulders' in pressure time series

### *4.2.1. Period-1 bubbling*

Period-1 bubbling is when the system is at its linear best. All bubbles produced are of the same size and a pearly string of bubbles emanates from the nozzle. This is observed at relatively low values of flow rate and voltage when there is minimal interaction between the succeeding bubbles.

**Figure 4.3** shows typical pressure trace of period-1 bubbling at low flow rates. Approximately 8 peaks are observed in 2 seconds giving a frequency of about 4Hz. In this plot the pressure traces are seen to be identical to each other with equal peak heights and peaks occurring regularly, equal distances apart in time. At low flow rates it is observed that a single train of bubbles is produced. All the bubbles in the train are equally sized and the train of bubble is seen to rise slowly, with all of the bubbles rising at the equal velocities. There is uniform interaction between the bubbles and bubble formation. The pressure trace output obtained for this case of bubbling is a series of identical peaks.

With a slight increase in flow rate or increase in voltage, the frequency of bubbling increases. A similar train of bubbles as the earlier case is seen only that the sizes of bubbles are different. But even now no interaction is seen between the bubbles (**figure 4.6a**).

When the control parameter is increased further, the frequency of bubbles increases further. But now interaction *is* observed between the bubbles and bubbles of two different sizes can be seen with the naked eye (**figure 4.6b**). The larger bubble seen to be the leading bubble and the smaller bubble is seen to be the trailing bubble. This marks the transition from period-1 to period-2 regime.

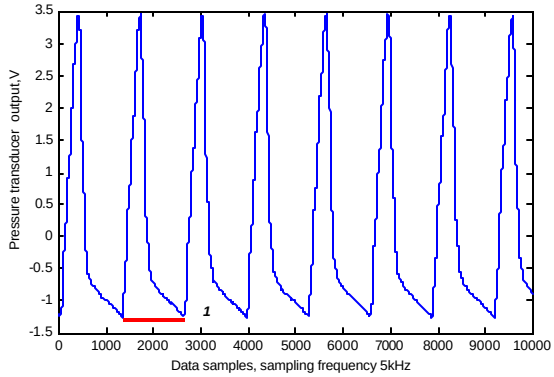


Figure 4.3. Pressure trace for period-1 bubbling

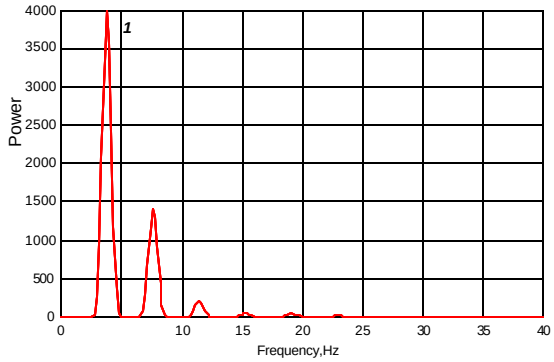


Figure 4.4. Power spectrum distribution for period-1 showing a single fundamental peak.

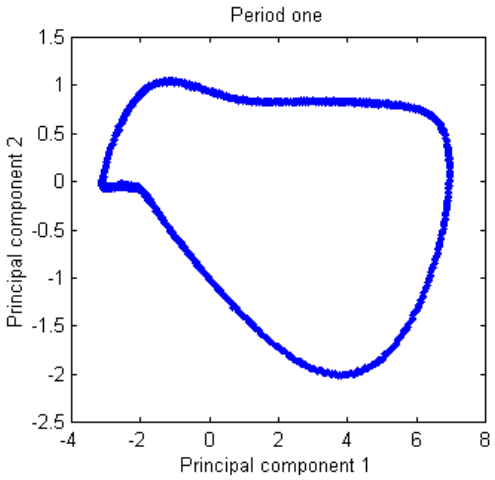


Figure 4.5. Phase space for period-1 bubbling showing a single-loop

(a) (b)

Figure 4.6. High speed images of slow bubbling.

(a) Period-1 bubbling. No interaction observed (b)Period-2 bubbling. Subtle interaction between bubbles observed

**Figure 4.4** shows the power spectrum distribution for period-1 bubbling. A peak at 3.8Hz is seen to be prominent. This gives the frequency of period-1 bubbling. This is the dominant frequency and the other smaller peaks seen in figure 4.5 at 7.6Hz, 11.4Hz and so on are the harmonics of this dominant frequency. If the period of the bubbles is calcuated, the mean calculated period is 0.2615s, which gives a frequency of bubbling as 1/0.2615s=3.8246Hz.

When the time-embedding algorithm is used to perform principal component analysis on the pressure trace time series, and the first two principal components plotted against each other, the result is a single loop in phase space. The system has a periodic component, which retraces itself in phase space as the system proceeds further in time. This is a characteristic of period-1. **Figure 4.5** depicts the phase space for period-1.

### *4.2.2. Period-2 bubbling*

In period-2 bubbling, the bubbles produced are alternately large and small in size. This mainly occurs because of the inter-bubble interactions. **Figure 4.7** shows a period-2 bubbling pressure trace.

Peaks of two distinctly different heights are observed. These correspond to the two different sizes of bubbles. The larger peak implies that the gas pressure forces in the nozzle along with the buoyancy forces needed to overcome the surface tension forces are larger and so a larger bubble is formed before bubble release occurs. The smaller peak suggests that resultant upward forces are stronger and overcome the surface tension forces faster, resulting in a smaller bubble and causing faster bubble release. The main reason period-2 occurs is the drag reduction caused by the wake left behind by the leading bubble, which sometime causes coalescence of the leading and the trailing bubble (**figure 4.10**). So now two different periods of bubble formation are

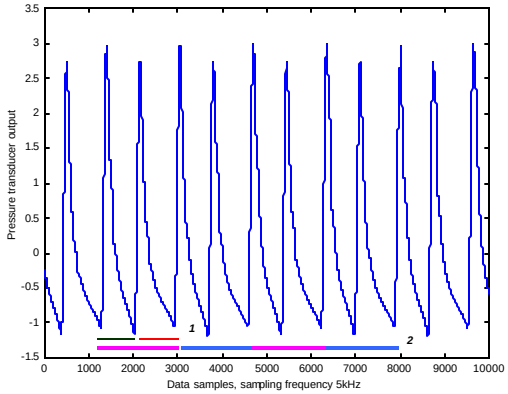


Figure 4.7. Pressure trace for period-2 bubbling

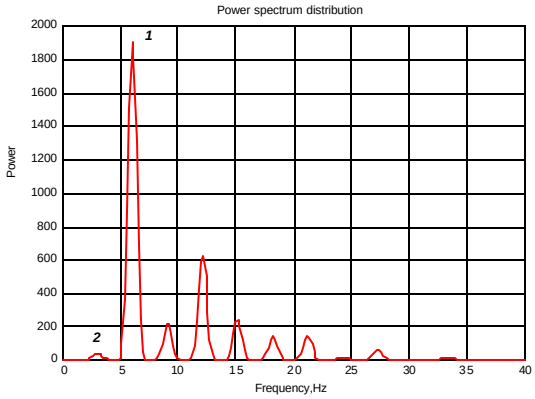


Figure 4.8. Power spectrum distribution for period-2 showing two fundamental peaks

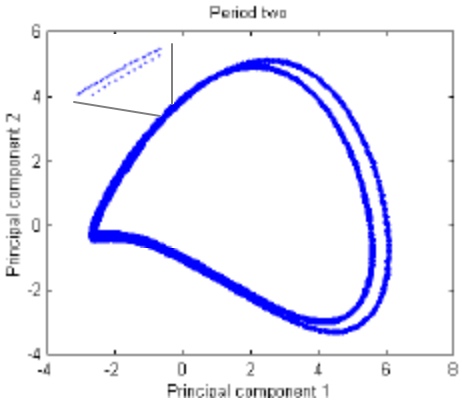


Figure 4.9. Phase space for period-2 bubbling showing two-loops

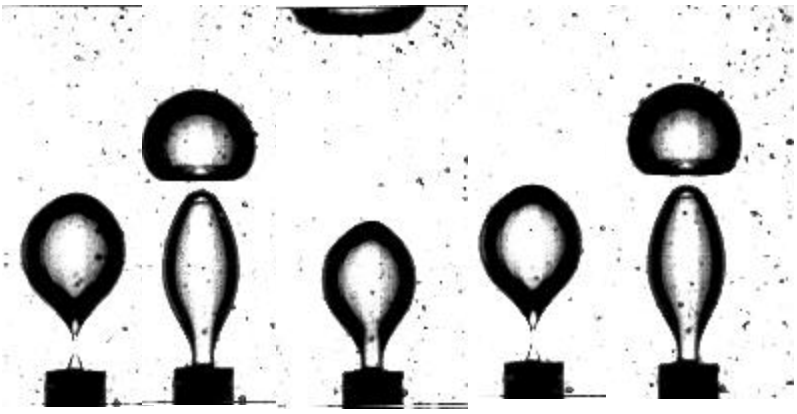

Figure 4.10. High speed images of period–2 formation of bubbles. Leading large bubble causes wake which forces an early release of the trailing bubble

observed. Comparison of this pressure trace with the one for period-1 bubbling shows that the peak- to-peak time intervals in the pressure trace for period-2 is smaller than that for period-1 due to higher flow-rate and bubble interaction. This is because the frequency of bubbling is higher in case of period-2 than in case of period-1. The plot shows about 12 peaks formed in 2 seconds giving a frequency of about 6Hz.

**Figure 4.8** shows a plot of the power versus the frequency of period-2 bubbling. Here we observe two different principal frequencies. One dominant peak is seen at 6Hz and another dominant peak is seen at 3 Hz

The average period of the bubbling was calculated to be 0.1803s (5.5458Hz) for the larger bubble and 0.1494s (6.6937Hz) for the smaller bubble. But in the power spectrum contrary to expectations of two peaks at the respective frequencies, only one peak at 6Hz, which is the average of the two bubbling frequencies, is observed. This is because the calculated period is the time of formation of bubble. But the maximum power occurs at the frequency at which both the events of bubble formation occur which is the average of the two frequencies. The whole cycle of formation of bubbles of two different sizes is occurring at one half the frequency at which the event for formation of the individual bubbles is occurring.

The Fourier transform sees the pressure trace as two separate period-one bubbling patterns occuring alternately, and a period-two bubbling pattern occuring at half the average bubbling frequency of the period-1 bubbles. This is illustrated in the pressure trace (figure4.7) with the two individual period-1's shown by red and black bars, and the period-2's being indicated by pink and blue. (Note that pink and blue bars are used to show the same pattern).

To summarize, period-2 is characterised by two peaks in the power spectrum distribution, the higher of which corresponds to the frequency at which the bubble formation occurs and the

other peak corresponds to the frequency at which the pattern of bubbling repeats itself. The average frequency of bubble formation is equal to the reciprocal of the average period between the bubbles and the frequency at which the period-2 bubbling pattern repeats itself is half of the average frequency. The maximum power occurs at the average frequency of bubble formation and the power at the frequency of the bubbling pattern is comparatively much lower.

Chaotic systems are best studied in phase space where bifurcations can be identified as soon as they occur. **Figure 4.9** depicts the trajectory in phase space the system follows in period-2 bubbling. The trajectory is seen to comprise of two loops. Even though the loops seem to merge as one at certain parts on the phase plot, the distinctness of the two loops is maintained, though a magnified scale is required to observe them.

### *4.2.3. Period-4 bubbling*

Period-4 bubbling can be thought of as a combination of two-period-2 bubbling patterns juxtaposed next to each other to form an overall sequence of four bubbles.

**Figure 4.11** shows the pressure trace for period-4 bubbling. Four distinctly different peaks are seen in the pressure trace. As the control variable is increased from period-2, the bubbling increases in frequency and consequently the period reduces. Further increases in the flow-rate lead to period-4 bubbling. A pattern of four different bubbles with alternate leading (large) and (trailing) small bubbles repeats itself. Here the pattern of 4 different peaks is subtle and special analysis tools like time return maps have to be used. It can be seen that the peak to peak height has reduced considerably and the frequency of the bubbles has increased. Approximately 18 peaks can be counted within the 2s time interval shown and the frequency of the bubbles is about 9Hz.

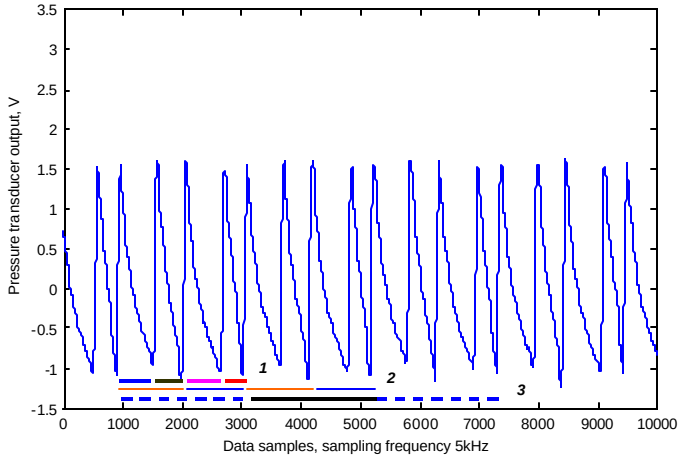


Figure 4.11. Pressure trace for period-4 bubbling

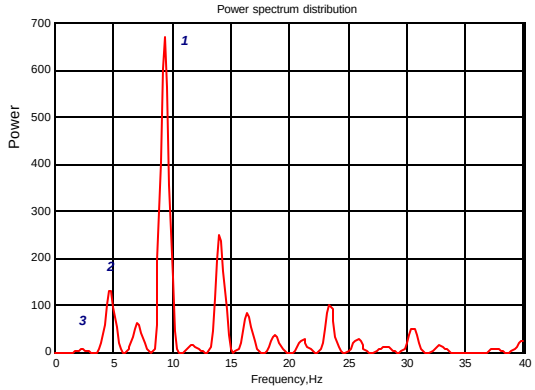


Figure 4.12. Power spectrum distribution for period-4 showing three fundamental peaks

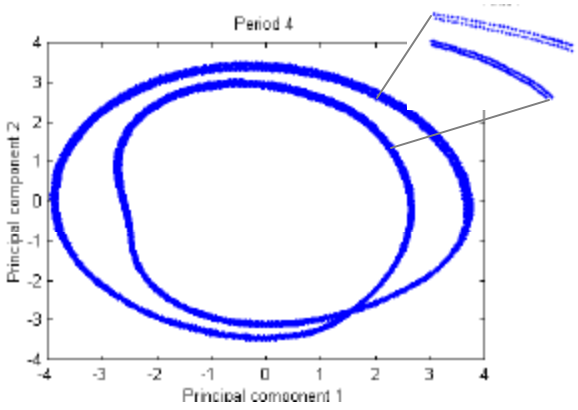


Figure 4.13. Phase space plot for period-4 showing four loops

**Figure 4.12** shows the plots for the power spectrum distribution for period-4 bubbling. In the power spectrum distribution, the dominant peak occurs at 9.4Hz, (peak 1) with two smaller peaks at 4.6Hz (peak 2), and 2.3Hz (peak 3). The peak at 7.1 Hz, and the rest of the peaks occuring in the spectrum are harmonics of these three frequencies. Period-4 bubbling occurs with formation of four bubbles of different sizes. So, the frequency of the formation of these four different bubbles dominates and is seen as a peak at 9.4Hz. But within each period-4 bubbling pattern, two period-2 bubbling patterns are observed.

Each of the two period-2 patterns are different from each other and this gives rise to period-4. The averge bubbling frequency of each of the two bubbling patterns shows up as the peak at 4.6Hz. These period-2 bubbling patterns occur faster than the whole cycle of period-4 bubbling and are slower than the frequency of the individual bubbles. The whole bubbling pattern of period-4 bubbling occurs at a frequency which is one half the frequency of period-2 bubbling and shows up as a very small peak at 2.3 Hz.

Period-4 is thus characterised by three peaks in the power spectrum distribution. The highest of the peaks corresponds to the frequency of bubble formation. This frequency is equal to the reciprocal of the averaged period between the bubbles. The lowest of the peaks corresponds to the frequency at which the overall bubbling pattern repeats itself. This frequency is equal to the reciprocal of the period of each cycle of four bubbles. The middle peak corresponds to the frequency at which the period-2 bubbling within period-4 bubbling repeats itself. This frequency is double the frequency of period-4 bubbling.

The phase plot for period-4 bubbling is shown in **figure 4.13**. On close examination, it can be seen tha there are four distinct loops in the phase plot, which could be mistaken for only 2

loops due to low resolution. The system traces each of the four loops as the bubbling proceeds. At least four peaks are required for the bubbling to close four loops in phase space.

### *4.2.4. Chaotic bubbling*

The description 'deterministically chaotic' (or chaotic, for short) is assigned to that class of physical and mathematical systems that exhibit bounded, irregular behavior due to sensitive dependence on initial conditions. Visually, chaotic bubbling is a regime wherein no truly repeating pattern can be traced. **Figure 4.14** shows the non-linear pressure time series for observations for chaotic bubbling.

**Figure 4.15** shows the power spectrum distribution of chaotic bubbling. To fully appreciate the spectrum of chaotic bubbling, a larger window size of 16,384 was used to reveal the details in the distribution, versus a window of 8,192 in earlier calculations. A similar window size was tried for each of the cases of periodic bubbling, but no significant difference in the power spectrum distribution was observed. In chaotic bubbling, bubbles of different sizes are formed in an aperiodic yet deterministic manner. So a spectrum of different bubbling frequencies exist and it becomes difficult to uniquely characterize chaos via power spectral analysis. But a qualitative indication of chaos can be obtained from the power spectral distribution, and possible chaotic behavior of bubbling can be predicted from the spectral observations. From the figure 4.15. we observe that now the peaks become less distinct and the bubble frequencies start to spread throughout the range of possible bubbling frequencies. Also, the power at the fundamental frequencies starts to decrease, indicating a larger spreading of power among other bubbling frequencies. it is important to note that certain frequencies was favored , and these frequencies show a distinct signature of period-4 bubbling.

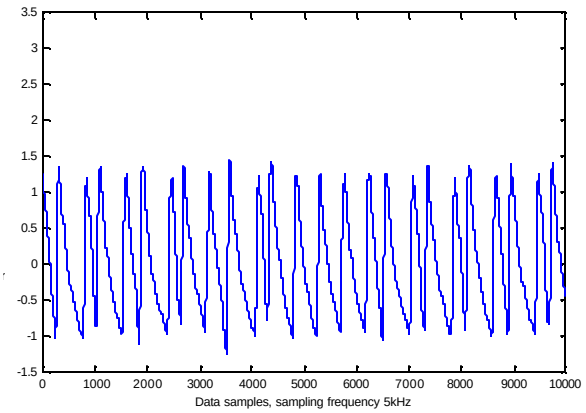


Figure 4.14. Pressure trace for chaotic bubbling

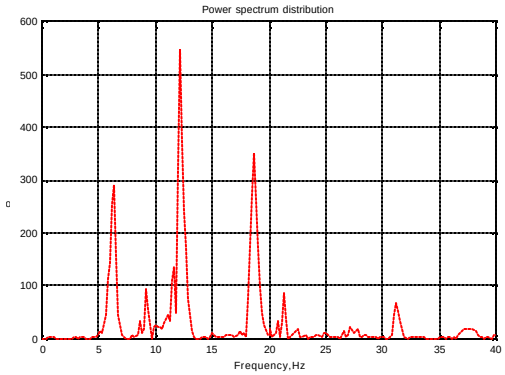


Figure 4.15. Power spectrum distribution for chaotic bubbling

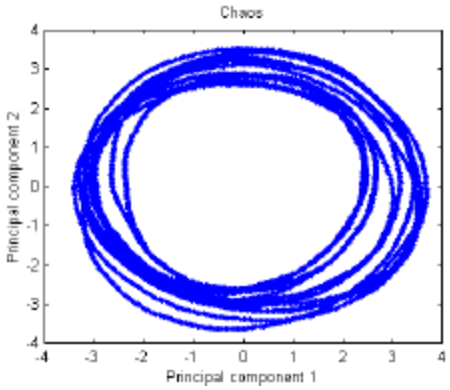


Figure 4.16. Chaos in phase space

In phase space (**figure 4.16**), the chaotic bubbling traces independent multiple loops, which outline a so-called strange attractor (unlike random systems which fill up the whole of the phase space).

In summary, periodicity can be diagnosed by analysis of the power spectrum distribution. Qualitative indication of chaotic bubbling is also possible, but the effectiveness of the power spectrum as a qualitative tool diminishes as chaos increases.

## 4.3. Effect of electrostatic potential on bubbling

To illustrate the effect of electrostatic potential on bubbling, a sample *'data slice'* at a nitrogen gas flow-rate of 334 cc/min was chosen. The data slice was taken at a *constant* flow rate increasing the voltage from 0 to 10,000 V in increments of 1000V. Each of the runs was plotted in a unique color with respect to the whole database, which was defined by an RGB (red-green-blue) vector formed by a constant, fraction of maximum voltage and fraction of maximum flow rate (RGB vector-[frac. max. voltage frac. maximum flow-rate 1]). All plots in this section has been plotted on the same scale for easy comparison.

### 4.3.1. Pressure traces

The non-linear pressure time series is the raw variable, available for analysis of the bubbling process. **Figure 4.17** shows pressure traces for bubbling at constant flow rate, but at various voltages. The data samples were taken at 2kHz, and a data length of 1 s has been shown. The voltage for each of the pressure traces has been mentioned as the title for each of the

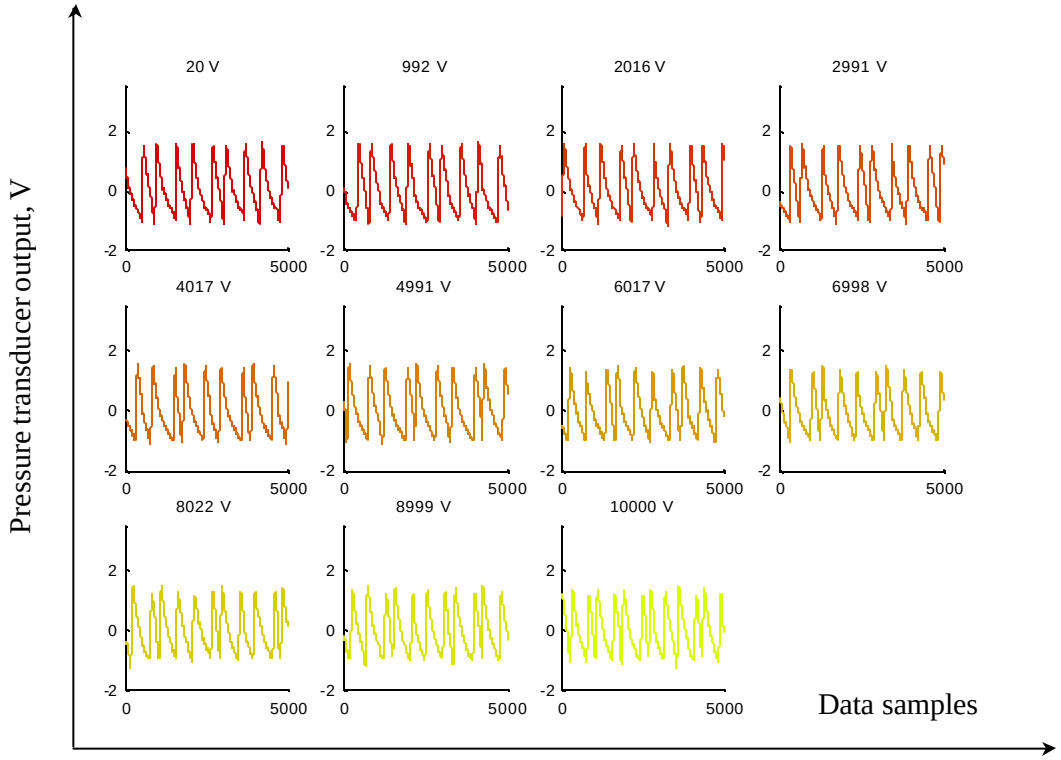


Figure 4.17. Pressure traces for bubbling with varying applied electrostatic potential, at a constant flow rate of 334 cc/min.

subplots. The voltage increases from left to right, and from top to bottom. The ordinate shows the output from the pressure transducer and the abcissa shows the data sample number.

A subtle difference in the pressure traces can be observed by visual inspection. The number of pressure trace peaks increase with an increase in applied electrostatic potential. It can be seen that the frequency of bubbling increases as the voltage increases.

*Note: The variation of pressure traces with increase in voltage is highly dependent on the nozzle diameter. In test runs carried out on with a nozzle diameter of 1mm internal diameter, a greater effect of electrostatic voltage was manifest (**figure 4.18-20**). This was attributed to the lower internal pressure in larger bubbles, allowing them to be distorted more by electrostatic forces.*

### 4.3.2. Periods of formation

Shifts in bubble formation period appear to be consistent with the onset of bifurcations. Using the pressure time series, the distance between the peaks was calculated and the corresponding time distance computed and plotted against the bubble index.

**Figure 4.21** illustrates the effect of applied electrostatic potential on the period of formation of bubbles. It can be observed that at the start of the run, the system is just into period-4. In the first plot, we observe three clearly distinct bubble periods, while closer inspection reveals that the longest period is actually split into two that are very close together. As the voltage is increased, period of formation of bubbles begins to decrease. The difference between the periods of formation also increases. This gives rise to four

distinctly different, but faster bubbles. Another interesting observation is that the smaller bubbles explain for most of the change in bubble size spectrum with change in electrostatic potential. This

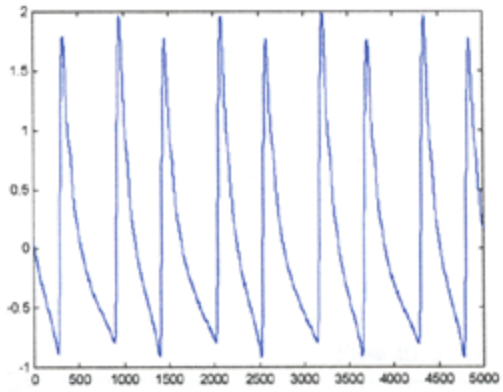


Figure 4.18. Pressure trace for 1mm ID nozzle at 0kV

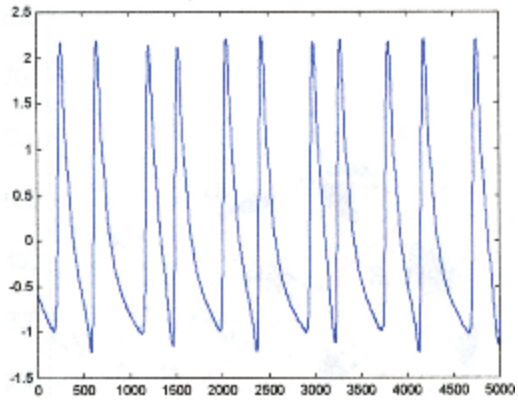


Figure 4.19. Pressure trace for 1mm ID nozzle at 5kV

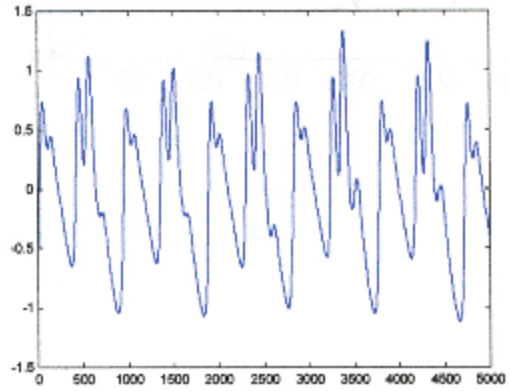


Figure 4.20. Pressure trace for 1mm ID nozzle at 7.5kV

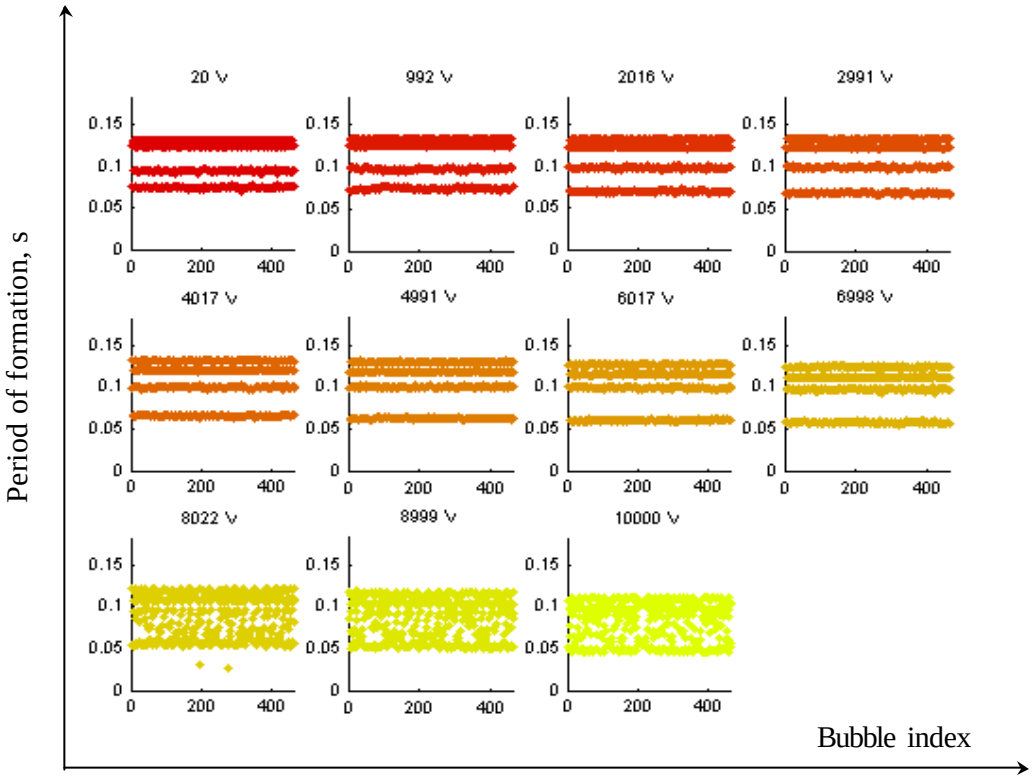


Figure 4.21. Period of formation of bubbles against bubble number, with varying applied electrostatic potential at a constant flow rate of 334 cc/min.

is because increase in electrostatic potential causes smaller bubbles to be released faster as compared to larger bubbles.

When the voltage is approximately about 3000V, four distinct bands of periods of formation are seen. As the voltage is increased further, the periods continue to get smaller and the bands move away from each other. Here it can be seen that the main difference occurs in the period of formation of the larger bubbles, which are seen at the top of the plots. So, from voltages from about 3000V up to 6000V, the system is said to be into well-defined period-4 bubbling.

At about 7000V, the bubbling system is seen to be on the verge of transitioning into more complex behavior approaching chaos. At this state when the system is extremely sensitive to ambient conditions and any disturbances however subtle are enough to affect the regime of the system in an exponential manner, either to cause the bubbling to revert to period-4 or to push it into chaos.

When the system approaches chaos, the periodicity of the system is lost and the bands seen in the period of formation plot become more and more fuzzy as the system approaches chaos. But during the transition into chaos, the system bears a signature of the earlier bubbling regime. Here (figure 4.21 subplot for 8022v) we can see that though the system enters chaos, there is a persistent memory of the original period-4.

### *4.3.3. Time return maps*

Time return maps are used for visualizing transitions in periodicity and chaos.. In a time return map, the period of every bubble is plotted against the period of the succeeding bubble.

**Figure 4.22** & **figure 4.23** illustrate the change in the periodicity of bubbles with an increase in the applied electrostatic potential at a constant flow rate, and vice versa. (For

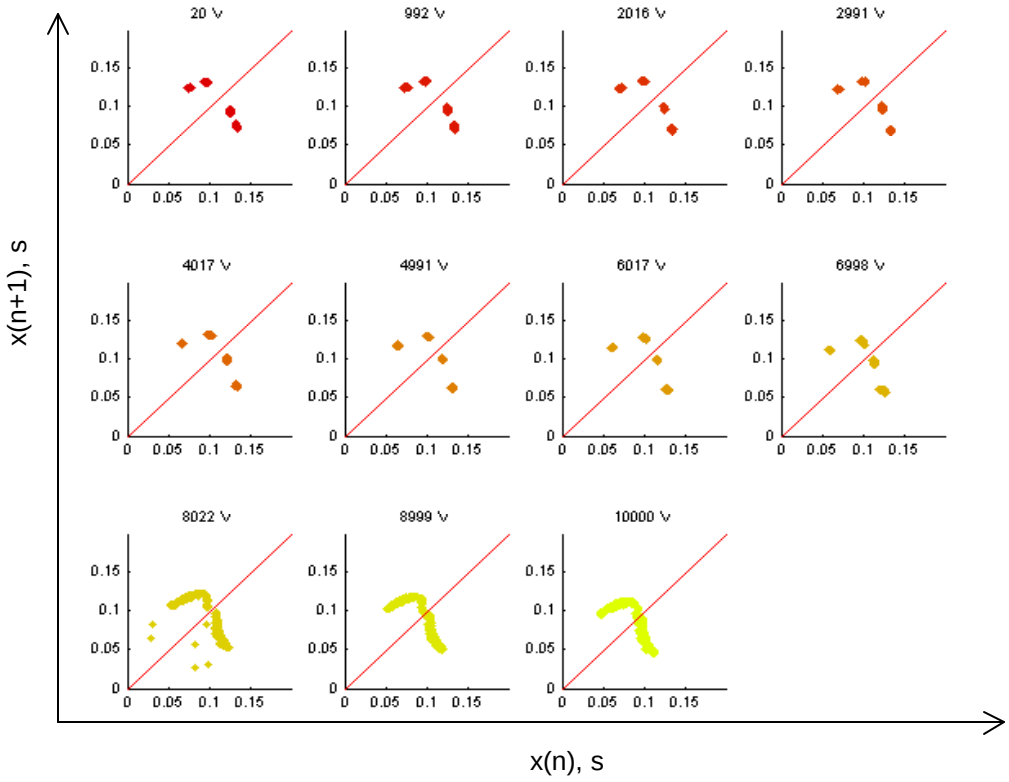


Figure 4.22. Time return maps with an increase in the applied electrostatic potential at a constant flow rate of 334 cc/min.

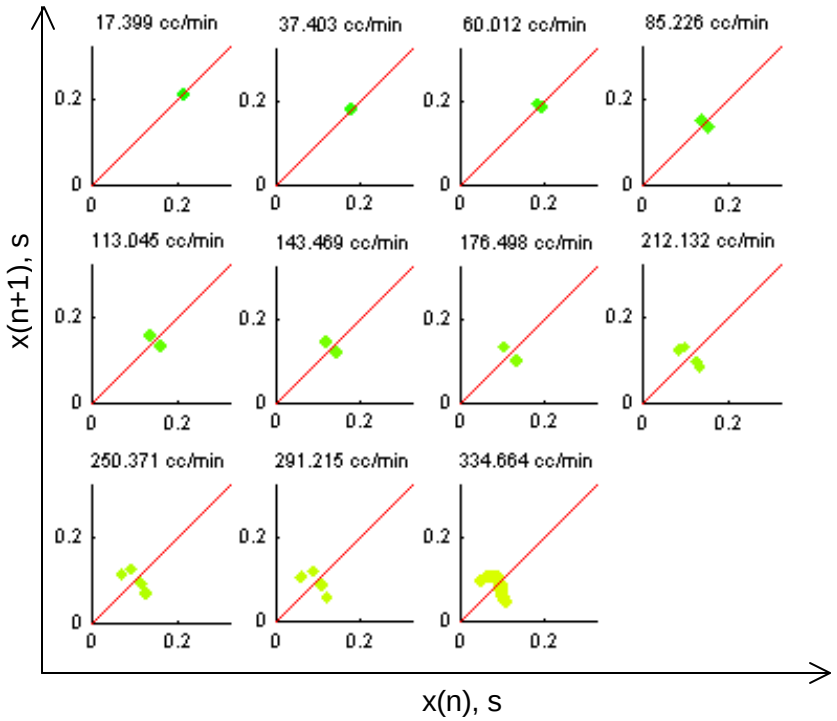


Figure 4.23. Time return maps with an increase in the flow rate at a constant applied electrostatic potential of 10,000 V.

comparison of the effect of electrostatic potential with the effect flow on the bubbling, **figure 4.24** shows all the plots from figure 4.22-23 on the same graph). At low values of applied electrostatic potential, the bubbling system is seen to have just bifurcated to a period-4 condition (indicated by the four distinct points on the plot). As the voltage is increased, the points on the time return map are seen to diverge from each other, indicating a shift into better-defined period-4. This happens because now the system has distinctly different periods of formation of bubbles. Between 3000-6000V, the system is seen to be in well-defined period-4 conditions. In the region from 3000-6000V, the change in either control variable, (flow rate or applied electrostatic potential), have to be substantial before the periodicity is changed. (Note: Progressive time return maps of an entire dataset are presented in appendix A)

At higher voltages, the system becomes more and more unstable and bifurcates into chaos at voltages beyond 7000V and higher. As the system bifurcates into chaos, the return map begins to fill in with the four distinct points becoming more and more indistinct. When the system is fully chaotic, all the points lie along a narrow ribbon-like strange attractor. The shape of the attractor is a system dependent phenomenon and characterizes a deterministic mapping relationship between successive bubble events. **Figure 4.25**(a) illustrates the time return map in 3 dimensions. It is worthwhile to note that the system reached this chaotic state at a *constant* flow rate, with an increase in the applied electrostatic potential. The return map plotted in this figure also gives information about the number of times the system revisited various regions on the return map. The colors vary directly with the intensity of points, with the lighter end of the spectrum indicating a maximum return frequency and darker colors indicating a minimum. The frequency distribution plot indicating the percentage of the total number of bubbles is shown in figure 4.25b.

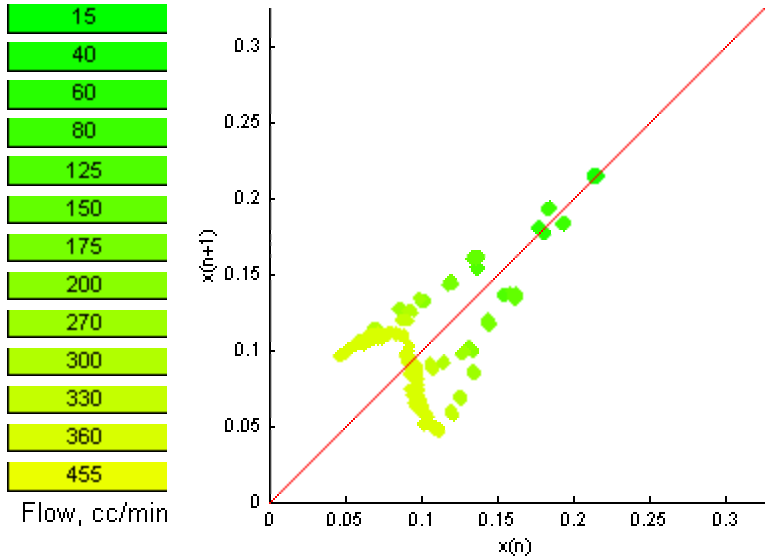


(a) Increase in flow-rate at constant voltage (10 kV)

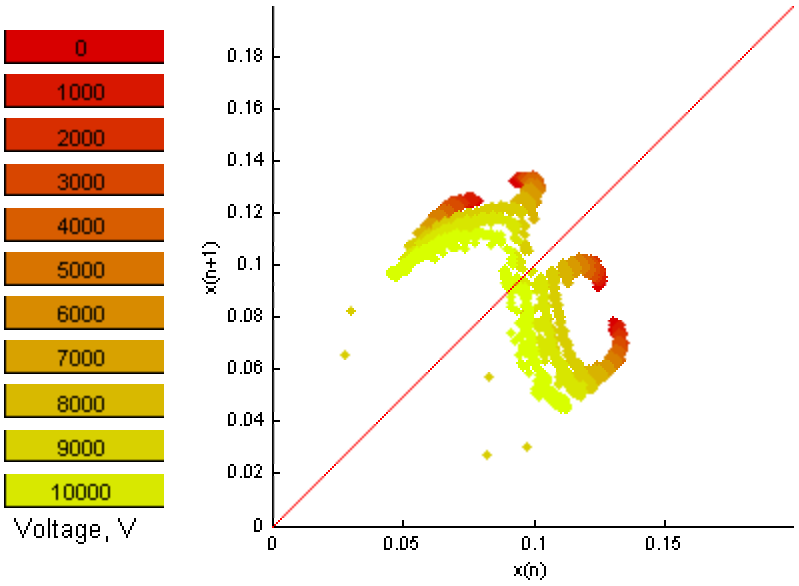


(b) Increase in voltage at constant flow-rate (334 cc/min)

Figure 4.24. Progressive time return maps with an increase in the respective control variable

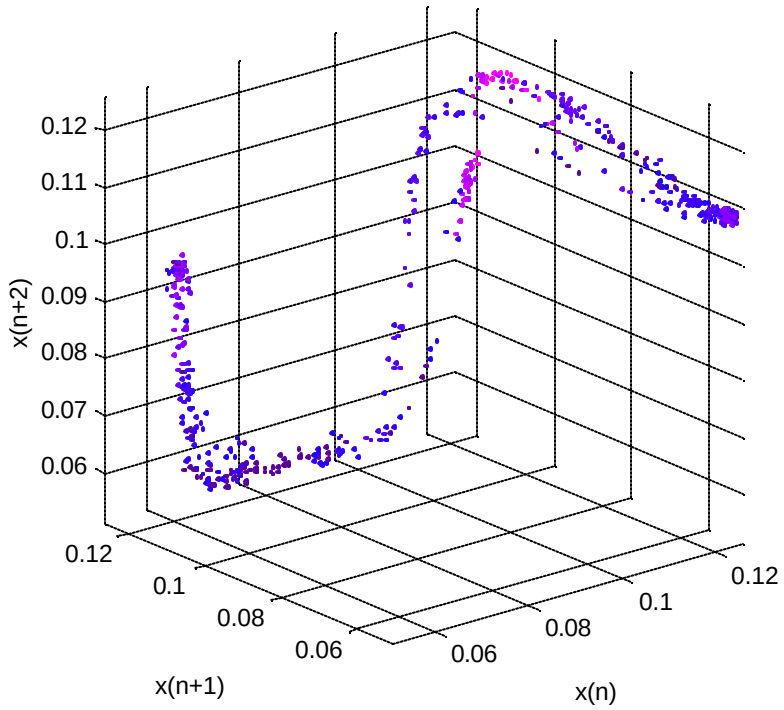


(a)

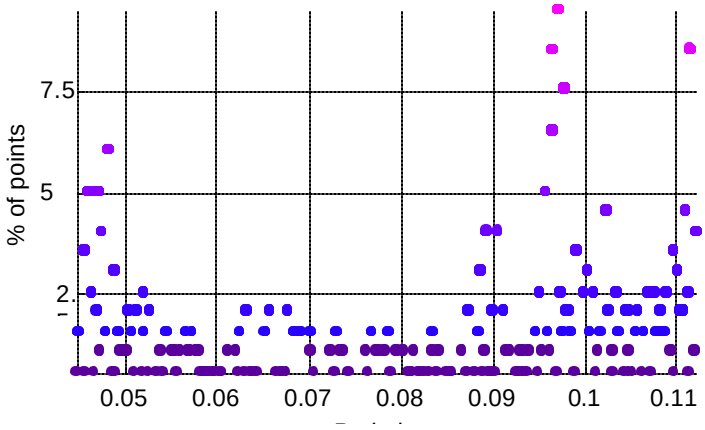


(b)

Figure 4.25. (a) Chaotic strange attractor in a 3-d time return map. The plot is presented as in intensity plot (b) with the lighter colors indicating greater number of visits.

### 4.3.4. Phase space analysis

At lower applied voltages, four distinct loops are seen in the phase space. As the system moves towards chaos, the phase space plot becomes more complex and less distinct. When chaotic, the system moves along several non-repeating trajectories in phase space, which are seen as a tangle of separate loops (**figure 4.26**).

### 4.3.5. Power spectrum distribution

Power spectrum analysis (**figure 4.27**) reveals power in a narrow range of frequencies at lower voltages when the system has higher periodicity. As applied voltage increases, the broadening bubble size distribution causes the peak height reduction, suggesting more distribution of power along a wider range of frequencies. An increase in the frequency of the dominant peak suggests an increase in the average bubbling rate. At bubbling regimes in chaos and near chaos, the power is spread along a range of frequencies causing an increase in the power at lower frequencies. As with flow changes, the power spectrum distribution though can only qualitatively suggest the occurrence of chaos.

### 4.3.6. Bifurcation diagram

Bifurcation diagrams illustrate the effect of the control variable on the periodicity of the system. By studying bifurcation plots, the dynamic state of the column can be qualitatively predicted and one or more parameters correspondingly adjusted to target a specific bubbling regime. Bifurcation analysis was used mainly to decide the optimum system state at which to employ control.

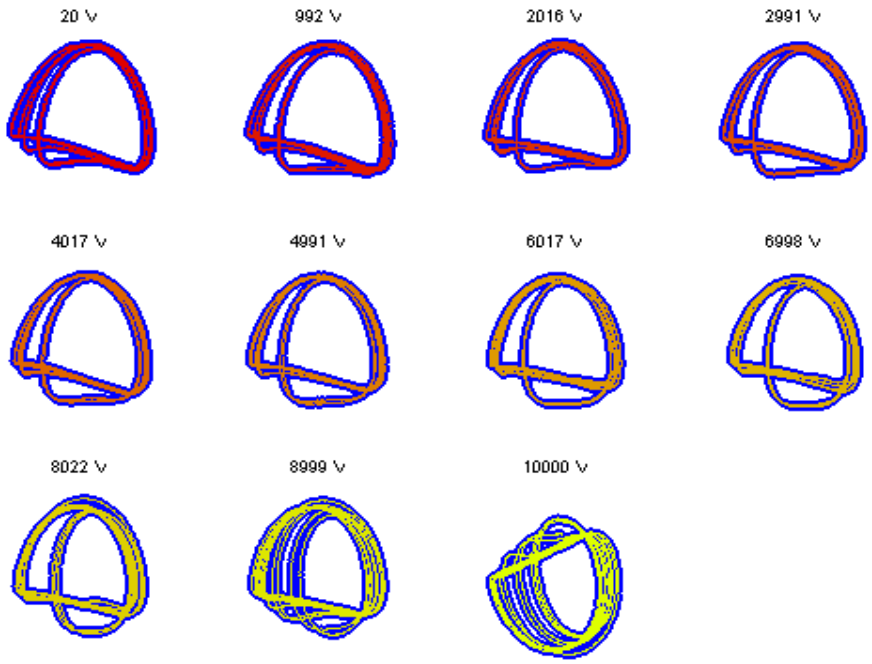


Figure 4.26. Phase space variations with varying applied electrostatic potential field strength, at constant flow rate of 334 cc/min *(note: All plots are on the same scale)*

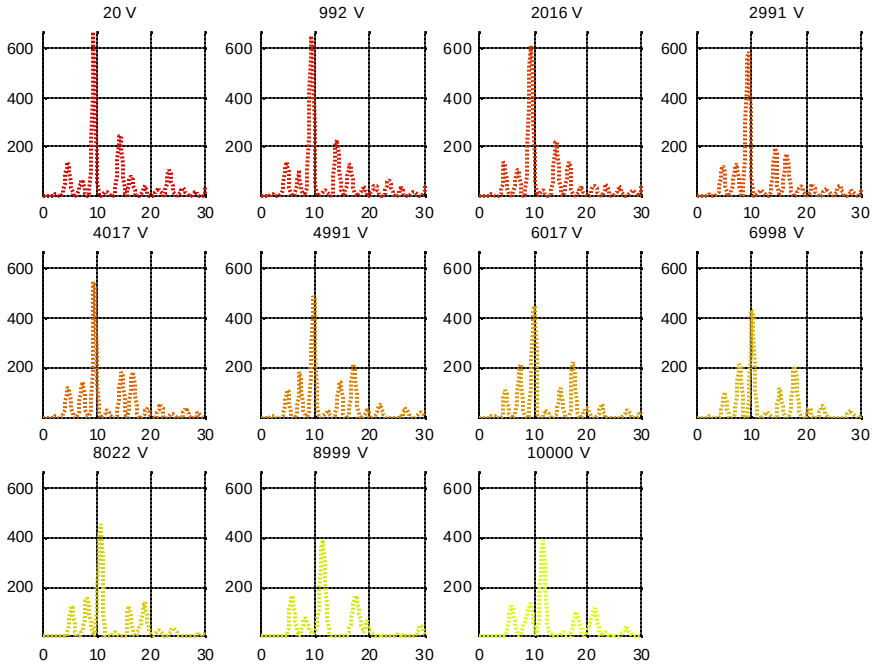


Figure 4.27. Power spectrum variations with varying applied electrostatic potential field strength, at constant flow rate of 334 cc/min

### *4.3.6.1.Bifurcation at constant voltage*

In **figure 4.28**, the flow rate has been kept constant at 334 cc/min, and the voltage was gradually increased in steps of 1000 volts from 0 to 10,000 V. Bifurcation of the bubbles with increase in electrostatic potential control variable is evident from this plot. At low values of the applied electrostatic potential, the system exhibits period-4. With an increase in voltage from left to right, the period of formation of bubbles decreases and at the same time the size distribution of the bubbles increases. Now, the system has four distinctly different bubbles forming. At higher values of applied voltage, the system starts bifurcating into chaos. When the system is chaotic, the periods of formation are almost continuously distributed along a wide band.

### *4.3.6.2.Bifurcation with voltage and flow*

In non-linear dynamics literature bifurcation maps involving changes to only one control parameter have widely been used. To analyze the effect of electrostatic potential in tandem with flow rate, similar bifurcation plots were made at different flow rates and plotted on the same plot to generate 3-dimensional bifurcation plots. It is seen that electrostatic potential alters the dynamics of the bubbling by decreasing the periodicity of the system. **Figure 4.29** gives the bifurcation of the system along the two axes and also marks the specimen system state to be studied in blue. This state is also highlighted in figure 4.28. It can be observed that with flow, the system is at a much higher value of

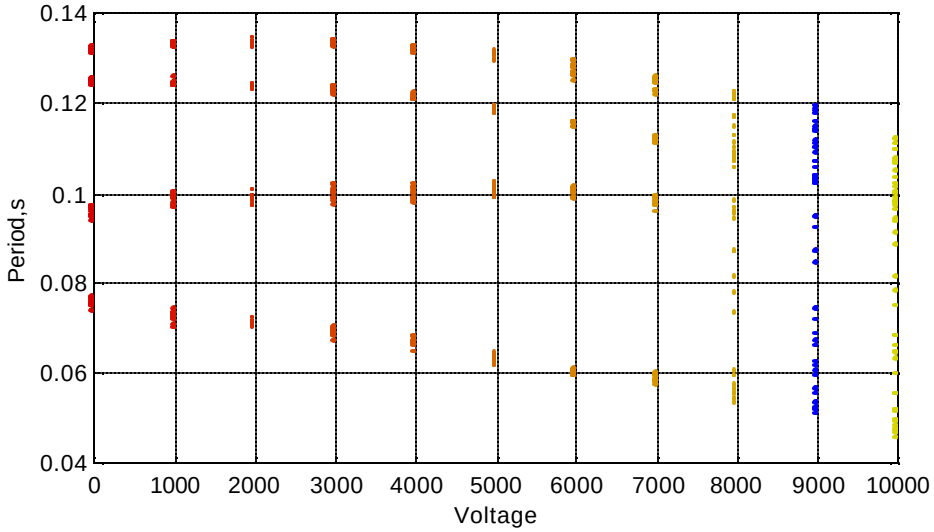


Figure 4.28. Bifurcation with applied electrostatic potential field strength, at constant flow rate of 334 cc/min

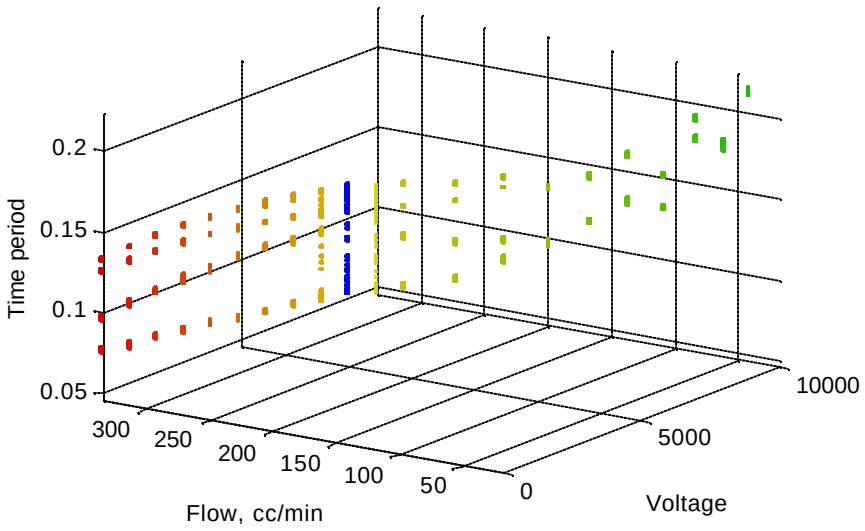


Figure 4.29. Position of a single run with respect to bifurcation with flow-rate and electrostatic potential in tandem

bubble formation at the top right corner of figure 4.29. Voltage on the other hand is much more subtle in its effect, which is manifest on the voltage axis.

### *4.3.6.3.Bubbling regimes in terms of dimensionless numbers*

Studying bubbling regimes in terms of dimensionless numbers give the operating conditions a more universal flavor. The dimensionless numbers chosen for study are the Tsuge flow-rate number (Tsuge, 1984) and the electric Bond number (Harris & Basaran, 1995; Shin & coworkers, 1997)

Tsuge's flow rate number is defined as

$$N_w = Bo.Fr^{0.5} \quad (1)$$

where

$$Bo = \frac{D_i^2 \rho g}{\sigma} \quad (2)$$

$$Fr = \frac{u^2}{D_i^2 \rho} \quad (3)$$

The Tsuge flow-rate number is a ratio of the buoyancy forces characterized by *Fr* and the surface tension forces, characterized by *Bo*.

Electric Bond number is defined as:

$$Be = \frac{d_i \varepsilon_a E^2}{\sigma} \text{ (Harris \& Basaran, 1995)} \quad (4)$$

The electric Bond number is a ratio of the electrostatic forces and the surface tension forces.

In order to study the collective effect of electrostatic and buoyancy forces, Shin and co-workers,(1997) suggested a modified Weber number which was the ratio of the sum of the electrostatic forces as compared to surface tension forces. This number is an indication of the total upward forces, which seek to release the bubble, as compared to the surface tension force which prevents the bubble release.

Modified Weber number is defined as:

$$We = \frac{d_i . \varepsilon_a E^2 + u^2 d_i \rho_a}{\sigma} \qquad (5)$$

The period of formation has been plotted against the voltage and the flow-rate in **figure 4.30** while in **figure4.31** the electric Bond number and Tsuge flow-rate number is used. One important observation in these two figures is that while the plots appear to be continuous in figure 4.30, a significant break in data is seen when the numbers are plotted on dimensionless axis in figure 4.31. This is because the dimensionless number definition contains a 'squared' term for the electrostatic field and flow rate for each of the two axes. This causes the values to shoot up as the absolute value increases. This also implies that the change in system state will be higher per unit change in control variable at higher values of the control variable.

The modified Weber number suggested by Shin and co-workers illustrates the combined effect of electrostatic potential and flow rate on the bubbling regimes (**figure 4.32**). Here the red markers indicate chaotic regimes and the colors with lower temperature indicate higher periodicity. The regime identification was done by an empirical 'regime-identifier' algorithm, which used ratios of peaks from the power spectral analysis. It is seen that period-1 is only seen

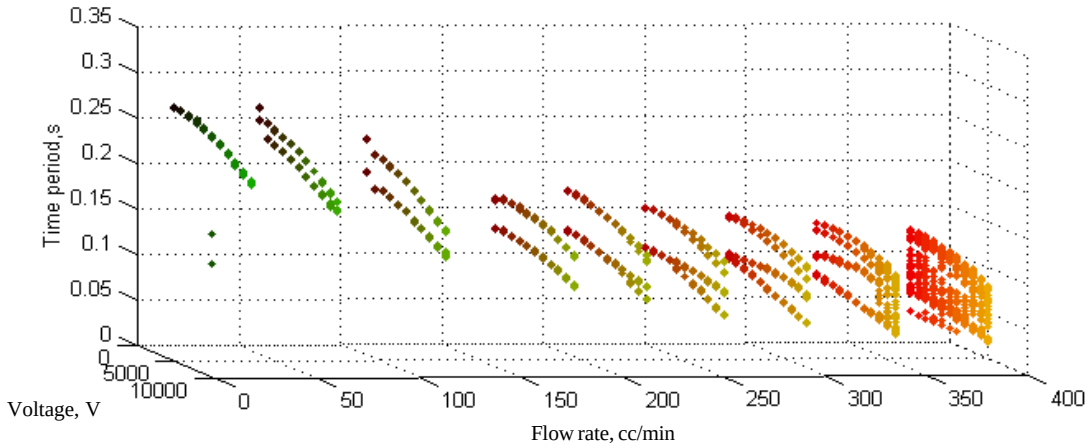


Figure 4.30. Bifurcation with flow and voltage

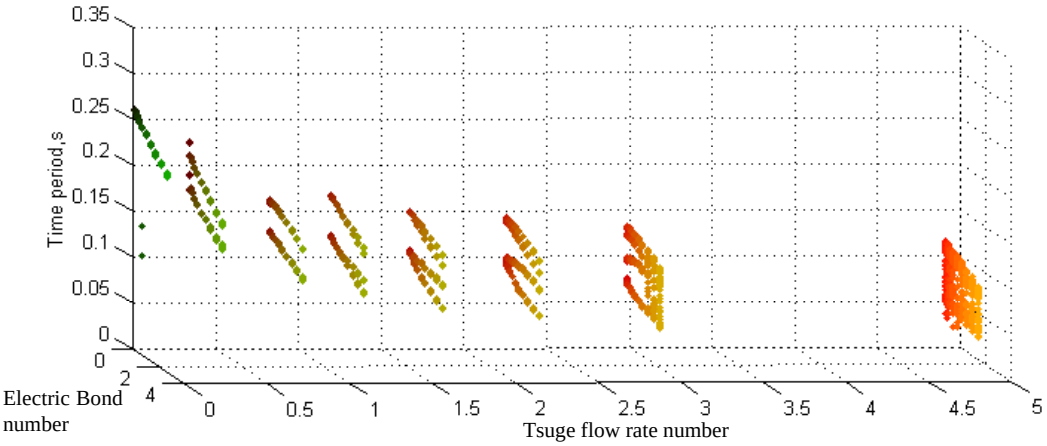


Figure 4.31. Bifurcation with flow and voltage against dimensionless axes

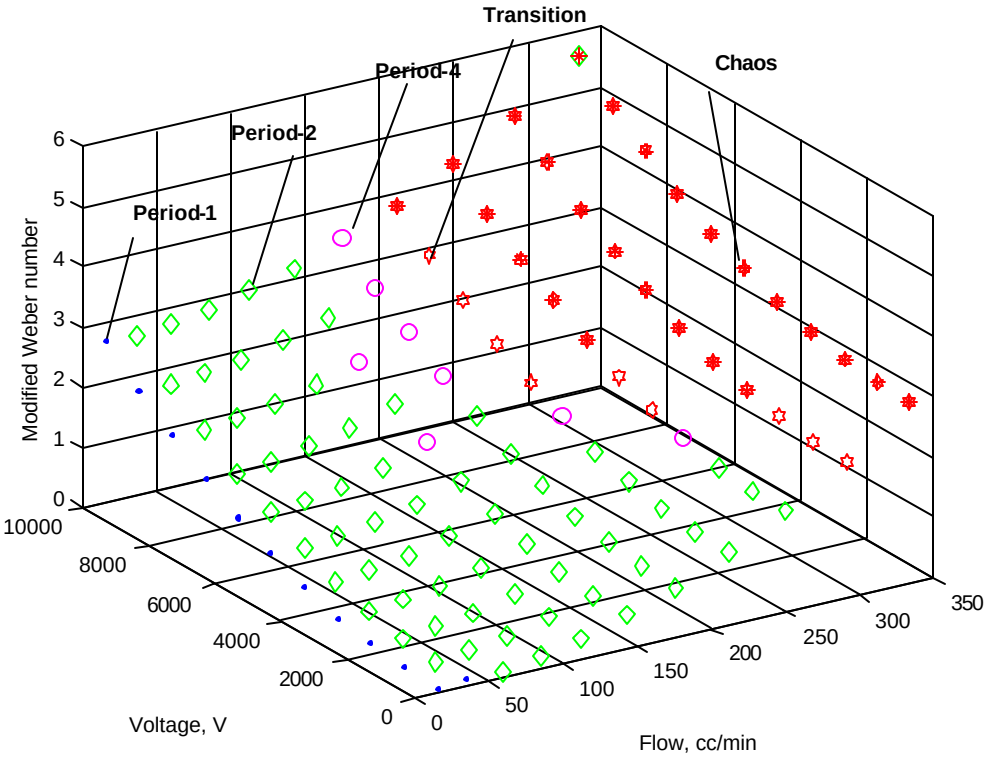


Figure 4.32. Bubbling regime plot in terms of the modified Weber number

at the low voltages and low flow rates. As either of the variables is increased, the bubbling regime passes through a period-2 and four before bifurcating into chaos. The bubbling regime cannot be predicted using the modified Weber number alone as the regime is also based on the ratio of the electrostatic and buoyancy forces. however the figure does show a clustering of regimes according to the modified Weber number.

The effective regimes of bubbling in terms of periodicity can be identified in **figure 4.33**, which gives the periodicity of the system in terms of the dimensionless flow rate number and electric Bond number. From figure 4.33, it can be observed that the increase in electric Bond number has a greater effect on the regime at values of higher Tsuge flow-rate numbers. At the Tsuge flow-rate number of about 1.7, increase in the electric Bond number causes change in bubbling regimes from period-2 into period-4 and finally into chaos.

The frequency of bubbling is affected by both the flow rate and the electrostatic potential. **Figure 4.34** shows the surface plot of the bubbling frequency as a function of the flow rate number and the electric Bond number. The plot also shows the projection of the surface plot onto the flow rate axis and the electrostatic axis, which can be termed as operating lines. The projection gives a qualitative idea about how the individual control variable impacts the frequency of bubbling. The projection on the flow axis shows the effect of the electrostatic potential. The linearity of the operating lines suggests the nature of the effect the flow. The electrostatic potential shifts the operating line from the lower extremity to the upper extremity, as the bubbling frequency increases with an increase in electrostatic potential. The linearity of the operating line is not affected to a large degree. This indicates that the electrostatic forces have a smaller effect on bubbling behavior than changing flow rateThe difference between the two operating lines gives the gain, which can be harnessed as a result of electrostatic potential as an additional control variable.

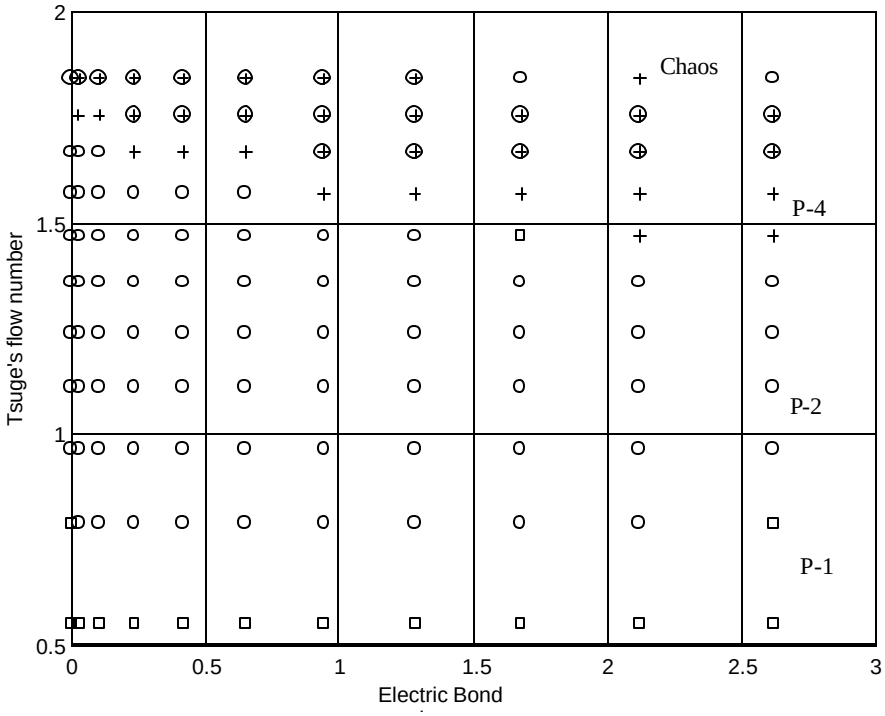


Figure 4.33. Bubbling regimes in terms of Tsuge's flow rate number versus electric Bond number

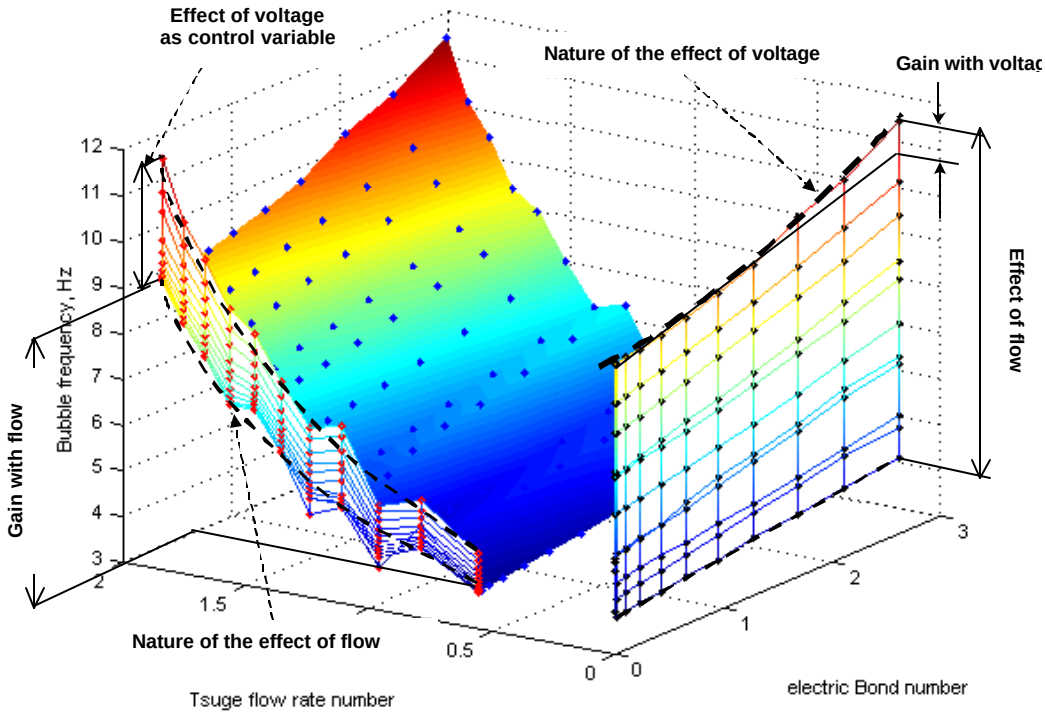


(a)

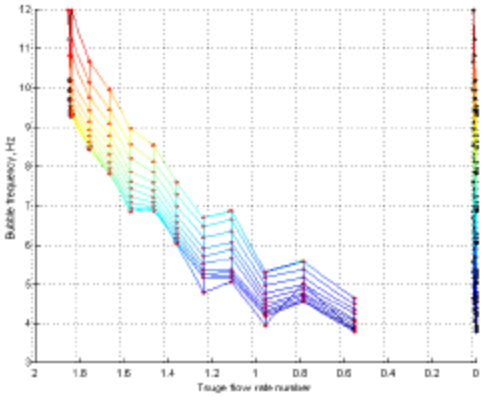

(b)

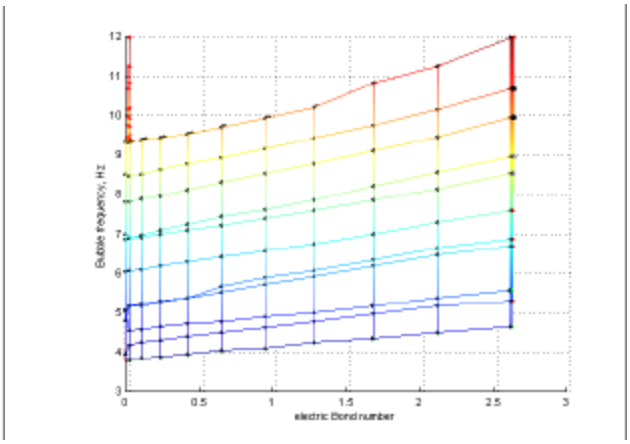

(c)

Figure 4.34. Frequency mapped as a surface plot against dimensionless flow-rate and voltage. (a) Surface plot of frequency of bubbling against dimensionless flow-rate and electrostatic potential (b) Projection of surface plot onto the flow-rate axis (Note: Abcissa is reversed) (c) Projection of surface plot onto the electrostatic potential axis

On the other hand, the operating lines on the electrostatic axes are affected by flow rate in stronger way. The operating line at low flow rates is close to being linear, where as at higher flow rates the operating line is curved suggesting more non-linear characteristics. Again the difference in the operating lines is the gain due to flow rate as the control variable.

Figure 4.34 suggests that to obtain maximum gain for control, the values of flow and electrostatic potential should be at the upper operating limit. But this also implies that the system will be chaotic and so any small changes in either of the control variables will be amplified exponentially. Well, that's where engineering and chaotic analysis comes together.